Available online at www.sciencedirect.com
SCIENCE DIRECT
Computer Vision and Image Understanding 102 (2006) 178–187
Computer Vision and Image Understanding
www.elsevier.com/locate/cviu

Multispectral image data fusion using POCS and super-resolution

Marcia L.S. Aguena, Nelson D.A. Mascarenhas *

Departamento de Computação, UFSCAR—Universidade Federal de São Carlos, Via Washington Luís, Km 235, 13565-905 São Carlos, SP, Brazil

Received 9 October 2003; accepted 13 January 2006
Available online 9 March 2006

Abstract

The problem of image data fusion coming from different sensors imaging the same object is to try to obtain a result that integrates the best characteristics of each one of those sensors. In this work, we want to combine the characteristics of multispectral (better spectral definition) and panchromatic (better space definition) images, using the bands from the satellites Landsat-7 (panchromatic) and CBERS-1—China-Brazil Earth Resources Satellite (four multispectral bands). The process proposes solutions using projection onto convex sets (POCS) techniques divided in two steps: (a) interpolated image processing, regularizing the block artifacts and using super-resolution techniques based on POCS and (b) synthesis, obtained by sequential and parallel projections or by the least squares method.

Keywords: Image data fusion; Remote sensing; Images synthesis; Image interpolation; Projections onto convex sets; Super-resolution

1. Introduction

The interpolation and the image data fusion are techniques used for compatibility and integration of images, from different sensors, of the same object. The interpolation tries to equalize the spatial resolution of the different data sources, while the data fusion combines the data obtained in the previous step, by providing an image with the best characteristics of each combined image. In the case of remote sensing, the fusion process synthesizes images with the spectral resolution of the multispectral images and the spatial resolution of the panchromatic image.

There are several methods for image data fusion described in the literature. One group of methods is based on the IHS transformation, which is used in a large variety of works as in Haydn et al. [1] and Brum [2]. Extensions of these ideas are based on projection techniques such as Principal Component Analysis and Projection Pursuit, as in Byrne et al. [3], Orlando et al. [4], and Petrakos et al. [5].

An interesting characteristic of multispectral image fusion, which is used by the filtering transformations and by the methods that use wavelets, is that the energy of the spectral characteristics is concentrated in the low frequencies, while the spatial characteristics (edges), are concentrated in the high frequencies. Béthume et al. [6] combined filters: a high-pass filter (HPF) applied to the panchromatic image and others based on the average of the local correlation (LMM) and on the variance and the average of the local correlation (LMVM) applied to the multispectral images to preserve their spectral characteristics. Aiazzi [7] used this concept to formulate a technique which combined the multispectral images bilinearly interpolated with the panchromatic band subtracted from its low frequencies. Gassemian [8] worked with the concept of MFB (Multirate Filter Banks) which divides the multispectral and panchromatic images in several frequency bands and combines them in the fusion process. Along these lines, some works applied the wavelet transform, as Gazerlli and Soldati [9], Núñez et al. [10], Scheunders [11], and Gomez et al. [12].

Mascarenhas et al. [13] proposed the simulation of a degraded SPOT panchromatic band by linear combination of multispectral bands as an example of a potential method to decrease the data rate on the link between the satellite and the ground. Latter Mascarenhas et al. [14] proposed a new data fusion method using bayesian statistical

* Corresponding author. Fax: +55 16 3351 8233.
E-mail addresses: aguena@dc.ufscar.br (M.L.S. Aguena), nelson@dc.ufscar.br (N.D.A. Mascarenhas).

1077-3142/$ - see front matter © 2006 Elsevier Inc. All rights reserved.
doi:10.1016/j.cviu.2006.01.001

estimation theory that uses the multispectral and panchromatic bands of SPOT satellite to generate ideal synthetic multispectral bands, close to 10×10 m spatial resolution.

The use of local correlation coefficients for data fusion was proposed by Hill et al. [15] and Zaniboni and Mascarenhas [16]. The latter method used locally adaptive correlation coefficients in the interpolation phase and, in the synthesis, a new method was proposed by performing a projection onto the linear subspace that defines the least squares solution of the synthesis problem.

This work uses a fusion model inspired in the work proposed in [14] and complemented in [16] for the fusion CBERS-1 × Landsat-7, using projection onto convex sets (POCS) in several steps of the overall process. Accordingly, Section 2 describes the necessary steps for the adaptation of the bayesian interpolation, originally proposed for the SPOT satellite, for the case CBERS-1 × Landsat-7. The solutions of the problems originated from this adaptation are presented in Sections 2.1 and 2.2 using POCS. Section 3 derives a new bayesian synthesis for the new situation. More specifically, in Section 3.1 a new POCS solution is presented for the synthesis by projection on the set of solutions of an underdetermined least squares problem, originally presented in [16] without using the POCS framework. In Sections 3.1, 3.2, and 3.3, the use of POCS to find numerical solutions for this problem with user selected characteristics demonstrate the versatility of these techniques. The experimental results are presented in Section 4 and the conclusions in Section 5.

1.1. Multispectral and panchromatic images

Multispectral images are obtained by sensors with narrow spectral bands, and for this reason, they have good spectral resolution, at the price of a poor spatial resolution On the other hand, panchromatic bands have poor spectral resolution, but better spatial resolution. In this work, we will treat the panchromatic band generated from the Landsat-7 satellite and the multispectral bands from the CBERS-1 satellite. All these bands and their characteristics are presented in Table 1. However, only some of these bands will be used (in highlight) in the fusion process.

1.2. Projections onto convex sets

In general, POCS techniques consist in modeling convex sets that represent the necessary restrictions so that a solution for a certain problem can be accepted. For each restriction, a projector on a convex set is determined and the projections starting from an initial value over the successive convex sets will converge to a point in the intersection of all the convex sets, which will be the solution of the problem.

POCS techniques in the present work were used in two different levels. First, by the identification of the proposed problem with models that have been utilized in similar situations [17], such as obtaining different solutions for underdetermined linear systems (Sections 3.1–3.3). Second, by reinterpreting different frameworks of existing applications (for example, reducing blocking artifacts in JPEG images and super-resolution in video sequences) for problems in this work (Sections 2.1 and 2.2).

Table 1
Images characteristics obtained by different sensors

Kind of image	Band	Spectral band (μm)	Spacial resolution (m)
Landsat-7			
Multispectral	1	0.45–0.52	30×30
	2	0.52–0.60	30×30
	3	0.63–0.69	30×30
	4	0.76–0.90	30×30
	5	0.55–1.75	30×30
	7	2.08–2.35	30×30
Panchromatic	1	0.50–0.91	12.5×12.5
CBERS-1			
Multispectral	1	0.45–0.52	20×20
	2	0.52–0.59	20×20
	3	0.63–0.69	20×20
	4	0.77–0.89	20×20

2. Interpolation

The interpolation developed to match the multispectral bands of the CBERS-1 with the panchromatic band of Landsat-7 was based on a method proposed by Mascarenhas et al. [14] and subsequently complemented by Zaniboni and Mascarenhas [16] for the SPOT multispectral bands matched to its panchromatic band. In that process, 3×3 neighborhoods from each one of the three SPOT multispectral bands, with 20×20 m resolution were used to linearly estimate four pixels of three new multispectral bands, with 10×10 m spatial resolution.

To use such method for the interpolation of the four multispectral bands of CBERS-1, of 20×20 m spatial resolution, with the panchromatic band of Landsat-7, of 12.5×12.5m resolution, due to the high value of the common minimum multiple between the spatial resolutions, large blocks of interpolation neighborhood were generated. Therefore, a neighborhood of 5×5 pixels, in each of the four multispectral bands generated interpolated blocks of 8×8 pixels in each of the four new multispectral bands, with a resolution of 12.5×12.5 m. To obtain a greater influence of the original neighborhood over the interpolated pixels, we stipulated a neighborhood of 7×7 pixels to obtain the same 8×8 interpolated pixels. Therefore, we use 196 pixels (7×7 in each of the four bands), denoted by vector y (196×1) to estimate 256 pixels (8×8 in four bands), denoted by vector $\hat{x}$ (256×1), as shown in Fig. 1.

Therefore, the nonhomogeneous linear estimator can be obtained by

$$\hat{x} = E[x] + \Sigma_{xy}\Sigma_{yy}^{-1}(y - E[y]), \tag{1}$$

where $E[x]$ is the statistical expectation, Σ_{xy} is the cross covariance matrix of x and y, and Σ_{yy} is the auto-covariance matrix of y. The method also assumes that the expected values do not change in the interpolation, therefore:

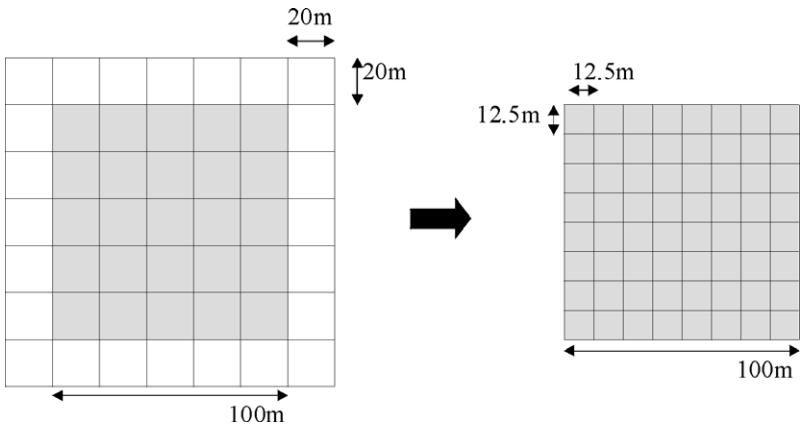

Fig. 1. Interpolation geometry: a set of 7×7 pixels with 20×20 m each will originate a set of 8×8 pixels with 12.5×12.5 m each.

$$E[x] = E[y]. \tag{2}$$

Under the separability assumption and lexicographic ordering, the covariance matrices will be given by:

$$\Sigma_{xy} = (C_h)_{xy} \otimes (C_v)_{xy} \otimes (\Sigma_S) \tag{3}$$

$$\Sigma_{yy} = (C_h)_{yy} \otimes (C_v)_{yy} \otimes (\Sigma_S). \tag{4}$$

The symbol $\otimes$ represents the Kronecker product of two matrices and h, v, and s represent, respectively, the horizontal, vertical, and spectral directions. Under the first order Markovian spatial correlation structure, matrices $(C_h)_{xy}$ and $\mathrm{e}(C_h)_{yy}$ are given by:

$$(C_h)_{xy} \begin{bmatrix} \rho_h^{i11} & \rho_h^{i12} & \cdots & \rho_h^{i17} \\ \rho_h^{i21} & \rho_h^{i22} & \cdots & \rho_h^{27} \\ \vdots & \vdots & \ddots & \vdots \\ \rho_h^{i81} & \rho_h^{i82} & \cdots & \rho_h^{i87} \end{bmatrix}, \tag{5}$$

$$(C_h)_{yy} = \begin{bmatrix} \rho_h^0 & \rho_h^1 & \rho_h^2 & \cdots & \rho_h^7 \\ \rho_h^1 & \rho_h^0 & \rho_h^1 & \cdots & \rho_h^6 \\ \rho_h^2 & \rho_h^1 & \rho_h^0 & \cdots & \rho_h^5 \\ \vdots & \vdots & \vdots & \ddots & \\ \rho_h^7 & \rho_h^6 & \rho_h^5 & \cdots & \rho_h^0 \end{bmatrix}, \tag{6}$$

where ρ_h is the correlation coefficient on the horizontal direction. The same structure is valid for $(C_v)_{xy}$ and $(C_v)_{yy}$, by substituting ρ_h by ρ_v. The values of ijk of the exponents of ρ are obtained by the distances between the original and interpolated centers and can be given by the equation

$$ijk = \left| \frac{(\mathrm{center}_j - \mathrm{center}_k)\mathrm{unit}_j}{\mathrm{unit}_k} \right|. \tag{7}$$

It is implicitly assumed that the distance between adjacent pixels on the original multispectral bands is unity. The specification of the correlation coefficients allows an adaptation of the method to the image local characteristics.

The covariance matrix Σ_S is the covariance matrix between the multispectral bands and will be given by:

$$(\Sigma_S) = \begin{bmatrix} \sigma_{11}^2 & \sigma_{12}^2 & \sigma_{13}^2 & \sigma_{14}^2 \\ \sigma_{21}^2 & \sigma_{22}^2 & \sigma_{23}^2 & \sigma_{24}^2 \\ \sigma_{31}^2 & \sigma_{32}^2 & \sigma_{33}^2 & \sigma_{34}^2 \\ \sigma_{41}^2 & \sigma_{42}^2 & \sigma_{43}^2 & \sigma_{44}^2 \end{bmatrix}, \tag{8}$$

where σ_{ji}^2 is the covariance between the bands i and j, and σ_{ii}^2 is the variance of band i.

The covariance matrix of the (256×1) vector $\hat{x}$, that gives the interpolated pixels, is easily found by:

$$\Sigma_{\hat{x}} = \Sigma_{xy} \Sigma_{yy}^{-1} \Sigma_{xy}^{\mathrm{T}}. \tag{9}$$

It should be observed that the (256×256) covariance matrix $\Sigma_{\hat{x}}$ carries not only spectral information, but also spatial information about the interpolated pixels.

We observe that, due to the large neighborhoods used in the 7×7 and 8×8 interpolations, the equations involve large matrices. Furthermore, as the matrices $(C_h)_{xy}$, $(C_h)_{yy}$, $(C_v)_{xy}$, and $\mathrm{e}(C_v)_{yy}$ are based on the distances between the centers of the interpolated pixels, their elements are also increased. For this reason, if the local correlation coefficients are high, there is oscillation in the amplitude of the generated 8×8 blocks, and blocking artifacts occur (see Section 4). To alleviate the problem, the following alternatives were pursuit:

(a) Use the interpolation with 7×7 blocks and reduce the ρ_h and ρ_v values, approximating them to zero. The negative side of this option is the decrease of the contrast in the image areas of higher roughness.
(b) Application of the algorithm for the reduction of the blocking effect, which was used in the images produced by a 5×5 neighborhood interpolation.
(c) Use interpolated images with an offset to reconstruct with the same resolution.

2.1. Blocking reducing algorithm

This algorithm is an application of the adapted algorithm described in [17,18] for the reduction of the resulting block artifact that occurs in the decoding of JPEG images.

The technique adopted for the problem solution was to impose the 8×8 block borders smoothness generated by the interpolation, in other words, to reduce the discontinuity in the junction of the gray tones along the columns and lines between the blocks. According to Fig. 2, to restrict the tone variations in the border areas, a limit is established for the differences of tones among the contiguous pixels, so that they do not surpass an established value E_i:

$$\|f_{8,i} - f_{9,i}\| \leqslant E_i \quad \text{with } i = 1, \ldots, 8. \tag{10}$$

Calling the border vectors and the accepted difference between the tones by:

$$\begin{aligned} f_8 &= (f_{8,1}, f_{8,2}, \ldots, f_{8,8})^{\mathrm{T}}, \\ f_9 &= (f_{9,1}, f_{9,2}, \ldots, f_{9,8})^{\mathrm{T}}, \\ E &= (E_1, E_2, \ldots, E_8)^{\mathrm{T}}. \end{aligned} \tag{11}$$

We can then define the restriction set and its projector as:

$$C = \{y : \|f_8^* - f_9^*\| \leqslant \|E\|\}, \tag{12}$$

$$\begin{aligned} f_8^* &= \alpha f_8 + (1-\alpha) f_9, \\ f_9^* &= \alpha f_9 + (1-\alpha) f_8, \end{aligned} \tag{13}$$

where α is obtained by

$$\alpha = \frac{1}{2}\left[\frac{\|E\|}{\|f_8 - f_9\|} + 1\right]. \tag{14}$$

The error vector E that is more adequate to the interpolated 8×8 block pixels limits can be obtained based on the differences of original image block of 5×5 pixels (E'), multiplied by matrix M:

$$E = M * E', \tag{15}$$

where

$$E' = \begin{bmatrix} |f'_{5,1} - f'_{6,1}| \\ |f'_{5,2} - f'_{6,2}| \\ |f'_{5,3} - f'_{6,3}| \\ |f'_{5,4} - f'_{6,4}| \\ |f'_{5,5} - f'_{6,5}| \end{bmatrix} \tag{16}$$

and $f_{5,i}$ e $f'_{6,i}$ for $i = 1, \ldots, 5$ are the pixel values of the limits of the 5×5 block from the original image that originated the interpolated 8×8 block. M is the weight matrix for the selection of the values of E', and their elements are computed based on the distances between the centers of the evaluated pixels, i.e.

$$M_{x,y} = \left[\left|\frac{(\mathrm{center}_x - \mathrm{center}_y)\mathrm{unit}_x}{\mathrm{unit}_y}\right|^{-1}\right]. \tag{17}$$

The process must be repeated for all vertical and horizontal limits, decreasing the blocking artifact.

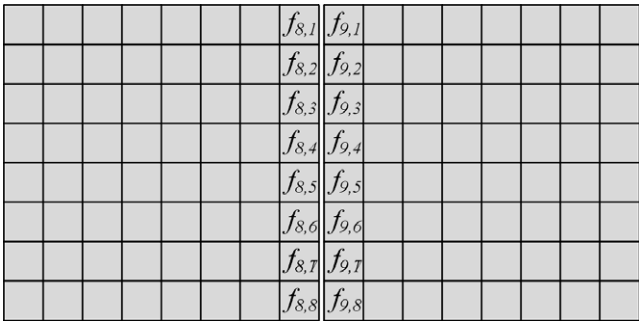

Fig. 2. The limits of the 8×8 blocks.

2.2. Image reconstruction

This algorithm is an application of the adapted algorithm described in [17,19], where a series of low-resolution images are taken by, say, a camera as it passes over a scene and the problem is to combine these low-resolution images into a single high-resolution image. This is the so-called super-resolution or resolution enhancement problem.

The whole adapted process described here is performed for the four multispectral bands simultaneously, although, to facilitate the understanding, it will be explained as if there were just one band. Now, we want to create several interpolated images of the same object, but with small offsets that result in different images. This occurs by the fact that if an offset is applied on the original image 5×5 division grid, the new interpolated image 8×8 division grid will not coincide with the older one as shown in Fig. 3.

The interpolated image, with the division grid beginning on coordinate $(1,1)$, is called S_1, the interpolated image with the division grid beginning on coordinate $(2,2)$ is called S_2, and so on until S_5, since we can observe that S_6 coincides with S_1, as shown in Fig. 4. The diagonal offset geometry was chosen, but another offset geometry could be chosen to obtain a larger number of interpolated images over the same original image (another possible offset may be on the vertical/horizontal directions). The chosen

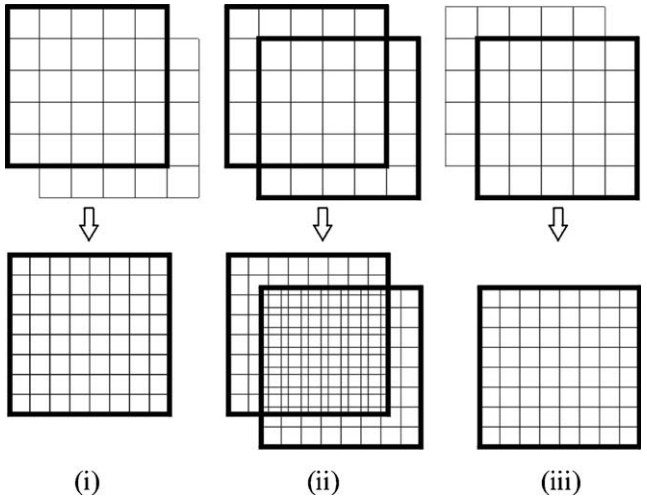

Fig. 3. A 5×5 block (i) moved one pixel to the right and down (iii), will generate an 8×8 block in the interpolation, that will not coincide with the one generated by the original (ii).

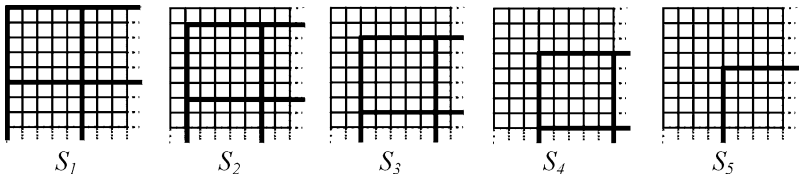

Fig. 4. Different offset division grids.

neighborhood size for interpolation does not interfere on this algorithm execution.

In that way, we have available $J = 5$ blurred images (BI) with dimension $M \times M$, and we will recover one with the same size. The blurred images are denoted by

$$\{d_j(m,n),\ m,n = 1,\ldots,M,\ j = 1,\ldots,J\}. \tag{18}$$

The image that will be reconstructed (RI) will be denoted by

$$\{f(k,l),\ k,l = 1,\ldots,M\}. \tag{19}$$

There will be M^2 unknown variables and JxM equations. Without noise, the relation between the blurred images and the reconstructed one is given by

$$d_j(x,y) = \sum_{k=0}^{M-1}\sum_{l=0}^{M-1} f(k,l)h_j(m,n,k,l), \tag{20}$$

where $h_j(m,n,k,l)$ is the point-spread function. From Eq. (20), we can see that the BI $d_j(m,n)$ are built-up by the weighted superposition of the $f(k,l)$ pixels. Assuming that the recovered image pixels are squares, as in Fig. 5, $h_j(m,n,k,l)$ will be the portion under the overlapping area of the pixels from jth BI, centered in (m,n) and the RI pixels centered in (k,l). $h_j(m,n,k,l)$ will be a weighted distribution of the contribution of the $d_j(m,n)$ from the jth BI to the pixel $f(k,l)$ from RI. From Eq. (20), we can estimate values (k,l) which minimize the error $\varepsilon(m,n,y)$, where

$$\varepsilon(m,n,y) \hat{=} d_j(x,y) - \sum_{k=0}^{M-1}\sum_{l=0}^{M-1} y(k,l)h_j(m,n,k,l). \tag{21}$$

We can say that the constraint set is

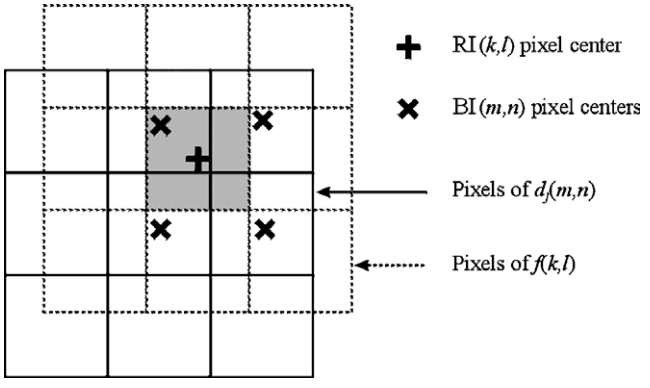

Fig. 5. Outline of Eq. (20), the contribution of the blurred image to the reconstructed image.

$$C_j(m,n) = \{y : \varepsilon_j(m,n,q) = 0\}. \tag{22}$$

And the projector is determined by

$$T = y^*(k,l) = \begin{cases} q(k,l) + \frac{\varepsilon_j(m,n;q)}{\|h_j\|^2} h_j(m,n;k,l) & \text{for } \varepsilon(m,n;q) \neq 0, \\ q(k,l) \ \text{ for } \varepsilon(m,n;q) = 0, \end{cases} \tag{23}$$

where $\|h_j\|^2$ is a Frobenius norm of matrix $[h_j(m,n;k,l)]$ and is given by

$$\|h_j\|^2 = \sum_{k=0}^{M-1}\sum_{l=0}^{M-1} h_j^2(m,n;k,l). \tag{24}$$

The solution is in $\cap_{m,n,j} C_j(m,n)$, and the recovering algorithm can be given by

$$f_{n+1} = P_{n,n} T f_n. \tag{25}$$

3. Synthesis

Similarly to the interpolation process, the synthesis process CBERS-1 × Landsat-7 used the synthesis method proposed in [14] to model the problem and adapting the spatial differences from the synthesis SPOT × SPOT. After the modeling of the problem, new solutions based on POCS were used, as alternatives to the bayesian synthesis proposed in [14] and to the least-squares projection method proposed in [16].

In the synthesis CBERS-1 × Landsat-7, we want to estimate ideal bands with spatial resolution of 12.5 × 12.5m, as the panchromatic band of Landsat-7. These bands should be spectrally close to the multispectral bands of CBERS-1.

The observation vector z given by the components $p_1,\ldots,p_{64}$ representing the 8×8 pixels of the original panchromatic image with spatial resolution 12.5×12.5 m and $y_1,\ldots,y_{100}$ the 5×5 pixels of the four original multispectral bandwidth spatial resolution 20×20 m is given by

$$z^{\mathrm{T}} = [p_1,\ldots,p_{64},y_1,\ldots,y_{100}]. \tag{26}$$

The vector of synthetic pixels f will have 256 components, 64 (8×8) for each one of the ideal bands and will be given by

$$f^{\mathrm{T}} = [f_{1,1},\ldots,f_{1,64},f_{2,1},\ldots,f_{2,64},f_{3,1},\ldots,f_{3,64},f_{4,1},\ldots,f_{4,64}]. \tag{27}$$

The vector f is locally related to the observed vector z by using an observation matrix H, to be described later, through a linear model, i.e.,

$$z = Hf. \tag{28}$$

From the original multispectral and panchromatic bands, we will synthesize ideal bands that are spectrally close to the original multispectral bands. In Fig. 6, we can notice a superposition between the multispectral bands and the panchromatic band.

The components of each row of the matrix H are defined by the fraction of the area under the ideal synthetic spectral sensitivity curves. The spectral relative response curves for each sensor will define the parameters of the matrix H where

$$A_i = \begin{bmatrix} \alpha_i & 0 & \cdots & 0 \\ 0 & \alpha_i & & \\ \vdots & & \ddots & 0 \\ 0 & & 0 & \alpha_i \end{bmatrix}_{64\times 64}. \tag{29}$$

and

$$B_i = \begin{bmatrix} B_i' \\ \vdots \\ B_i' \end{bmatrix}_{25\times 1} \tag{30}$$

with $i = 1, \ldots, 4$ and

$$B_i' = \begin{bmatrix} \beta_{i1} & \cdots & \beta_{i1} \\ \beta_{i2} & \cdots & \beta_{i2} \\ \beta_{i3} & \cdots & \beta_{i3} \\ \beta_{i4} & \cdots & \beta_{i4} \end{bmatrix}_{4\times 64} \tag{31}$$

and

$$\alpha_i = \frac{P \cap S_i}{P}, \tag{32}$$

where P is the area under the panchromatic band spectral response curve, S_i is the area under the ideal ith band spectral response curve, $i = 1,2,3,4$, and $P \cap S_i$ is the area under the minimum of the panchromatic band spectral response curve and the ideal ith band spectral response curve, $i = 1,2,3,4$, and

$$\beta_{jk} = \frac{25}{64}\frac{x_{sk} \cap S_j}{x_{sk}}, \tag{33}$$

where x_{sk} is the area under the kth multispectral band spectral response curve. $x_{sk} \cap S_j$ is the area under the minimum of the kth multispectral band spectral response curve and the ideal jth band spectral response curve, $k = 1,2,3,4$ and $j = 1,2,3,4$. We make the assumption of an infinite spectral response of the ideal synthetic bands within their limits. The factor 25/64 takes into account the different resolutions of the multispectral bands (20×20 m) and the synthesized bands (12.5×12.5 m).

As was observed before, system (28) is underdetermined, with an infinite number of solutions. The projection methods will be applied to obtain one of the possible solutions to this system.

3.1. Projection by the least-squares method

The method proposed by Zaniboni and Mascarenhas [16], as an alternative to the bayesian synthesis, was given by the solution of the system of Eq. (28), through the projection of the interpolated images on the vector subspace defined by the solution of the underdetermined least squares problem. In this work, we reinterpret this solution as a POCS technique. Fig. 7 illustrates the figure of a "gutter," which represents the residual of the underdetermined least-squares problem. The projection of the bottom of the "gutter" is the set of infinite solutions of this problem. A reasonable choice of the solution is so select the closest point over the set of infinite least-squares solutions that is closest to the interpolated multispectral images, since the ideal bands are selected over the spectral response of the multispectral bands.

The projection of x_0 (interpolated multispectral images) on the set CMQ in Fig. 7 can be obtained in a single step and it can be given by the projector [17]:

$$f = x_0 - H^{\mathrm{T}}[HH^{\mathrm{T}}]^{-1}(Hx_0 - z). \tag{34}$$

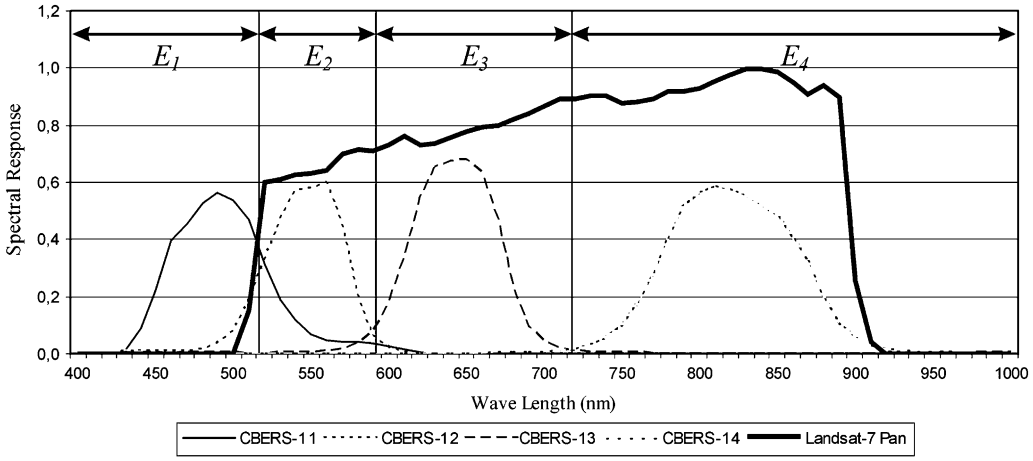

Fig. 6. Relationship among the CBERS-1 multispectral bands, the Landsat-7 panchromatic band and the ideal synthetic bands E1, E2, E3, and E4.

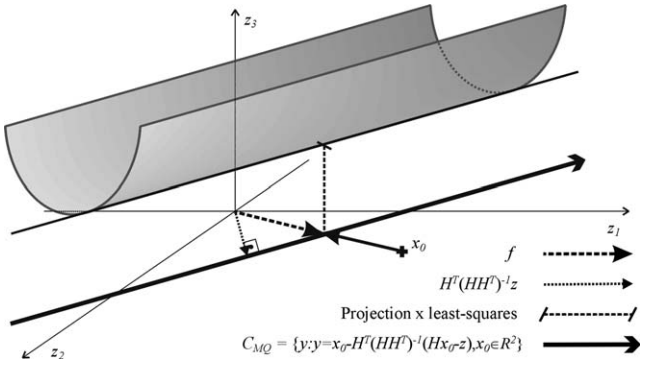

Fig. 7. A "gutter," which represents the residual of the underdetermined least squares problem.

The POCS method for the solution of linear systems substituted the bayesian method through the least squares solution.

As was observed before, system (28) is underdetermined, with an infinite number of solutions. Alternative projection (POCS) methods will be applied in the next sections to obtain one of the possible solutions to this system, offering greater flexibility in the choice of the solution.

3.2. Sequential projections on matrix H lines

The solution of Eq. (28) found by using POCS methods is a linear system solution, in other words, obtained by sequentially projecting the initial value onto sets, represented by the equations described by the rows of the H matrix, until arriving to a limit value in the intersection of the constraint sets. The set S_i and the projector used for each row of H are given by the equations:

$$S_i = \{f : \langle H_i, f\rangle = z_i\}, \tag{35}$$

$$Ps_i = \begin{cases} f & \text{if } f \in Si, \\ f - \frac{\langle H_i, f\rangle - z_i}{\|H_i\|^2}, \end{cases} \tag{36}$$

where H_i is the vector described by the ith row of H matrix and z_i is the ith element of vector z. The solution is obtained by the iterative application of the following algorithm until its convergence

$$x_{k+1} = Ps_m \cdots Ps_2 Ps_1 x_k, \quad k = 0, 1, 2, \ldots \tag{37}$$

System (28) has an infinite number of solutions and this one found by the convergence of algorithm (36) is just one of them. The solution found is the nearest one to the last set in the algorithm projection. The flexibility of the method is due to the fact that there is no constraint about the order of the lines of H projections. So, if we start the algorithm on the last line and go up to the first line, as following:

$$x_{k+1} = P_1 P_2 \cdots P_m x_k, \quad k = 0, 1, 2, \ldots \tag{38}$$

The solution found will be nearest to the constraint sets of the first lines of matrix H, which are derived by the relationship between the panchromatic bands and the ideal synthetic bands.

3.3. Parallel projections

The parallel method consists in simultaneously projecting the initial value onto all lines of matrix H, and obtaining the average value of the projections. This method can also be executed by a weighted average of the projections, making possible to adjust the solution characteristics, close to the original multispectral or panchromatic image. We will use the concept of weighted square norm, defined by the operator $\|\!|\cdot|\!\|^2$ and by the positive constants $w_1, w_2, \ldots, w_n$, such that $\sum_{i=1}^{n} w_i = 1$ and

$$\|\!|X|\!\|^2 = \sum_{i=1}^{n} w_i \|x_i\|^2. \tag{39}$$

The idea of parallel projection onto the lines of H is to project an initial value onto all lines of H (hyperplanes), and to calculate the projections mean (weighted or not). To obtain this projection, we will start by defining two sets:

$$C = \{Y : Y = (y_1, y_2, \ldots, y_m) \text{ with } y_i \in C_i \text{ for } i = 1, \ldots, m\} \tag{40}$$

and

$$D = \{Y : Y = (y_1, y_2, \ldots, y_m) \text{ for } y_1 = y_2 = \cdots = y_m\}. \tag{41}$$

The projector set C is given by

$$P_C Y = (P_1 y_1, P_2 y_2, \ldots, P_m y_m), \tag{42}$$

where P_i, $i = 1, \ldots, m$ is the projector defined by Eq. (36).

For an arbitrary vector $X = (x_1, x_2, \ldots, x_n)$ and $Y = (y_1, y_2, \ldots, y_n) \in \mathrm{C}$, we will seek the nearest possible point Y^* to X, although using a weighted square norm. Therefore

$$\|\!|X - Y|\!\|^2 = \sum_{i=1}^{n} w_i \|x_i - y_i\|^2. \tag{43}$$

Taking the gradient with respect to y and setting it equal to the zero vector, we will have

$$Y^* = P_D X = \left(\sum_{i=1}^{n} w_1 x_1, \sum_{i=1}^{n} w_2 x_2, \ldots, \sum_{i=1}^{n} w_n x_n \right). \tag{44}$$

We can observe that if the weights are equal, the solution will be equidistant to all projection sets. The final result is obtained by the convergence of the algorithm:

$$Y_{n+1} = P_D P_C Y_n. \tag{45}$$

4. Experimental results

4.1. CBERS-1 × Landsat-7 interpolation

The largest problem faced in the fusion of the CBERS-1 multispectral and Landsat-7 panchromatic images was the incompatibility of the spatial resolutions, of 12.5×12.5 m of the panchromatic image and

20×20 m of the multispectral images. The solution found was to interpolate blocks of 5×5 pixels to generate others of 8×8. Being four the multispectral bands (C1, C2, C3, and C4) of CBERS-1, the method works with blocks of $5 \times 5 \times 4 = 100$ pixels to interpolate other $8 \times 8 \times 4 = 256$, generating matrices and vectors of high dimensions. Due to the size of the blocks, the blocking artifacts occur. Fig. 8 shows the four multispectral bands of CBERS-1, in images of 140×140 pixels, covering an area of 1024 km^2 and Fig. 9 displays the panchromatic band of Landsat-7, in an image of 224×224 pixels, covering the same area of the multispectral bands.

The interpolation model with 5×5 neighborhood does not allow the neighborhood of the 5×5 block to influence the 8×8 block of the interpolation. If we increase the neighborhood to be interpolated, another blocking artifact will affect the 8×8 interpolated blocks, generated by the numeric differences of the exponents of the matrices $(C_h)_{xy}$ and $(C_h)_{yy}$. That artifact is shown in the second line of the Fig. 10 using an interpolation with 7×7 blocks. To soften the problem, we can decrease the value of the local correlation coefficients ρ_v and ρ_h approaching zero, as shown in the third line of Fig. 10. On the other hand, with the decrease of the values ρ_v and ρ_h, the contrast generated by the adaptability of the correlation coefficients in rough areas also decreases. An alternative for the domino of problems in the CBERS-1 × Landsat-7 interpolation is to process the images. The first proposed solution was the algorithm of blocking reduction imposing a contrast limit in the areas of limits of blocks. The result of that algorithm is in the fourth line of Fig. 10.

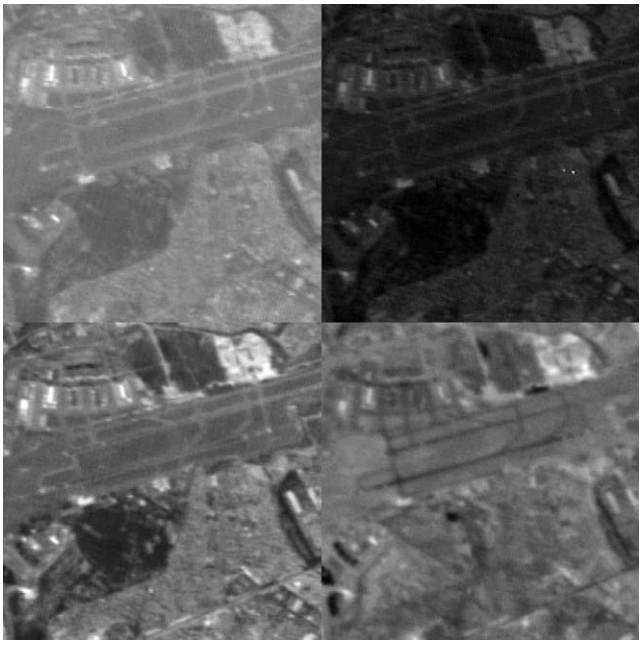

Fig. 8. CBERS-1 original multispectral images: C1, above left; C2, above right; C3, below left, and C4, below right. All with 140×140 pixels.

Fig. 9. Landsat-7 panchromatic image, with 224×224 pixels.

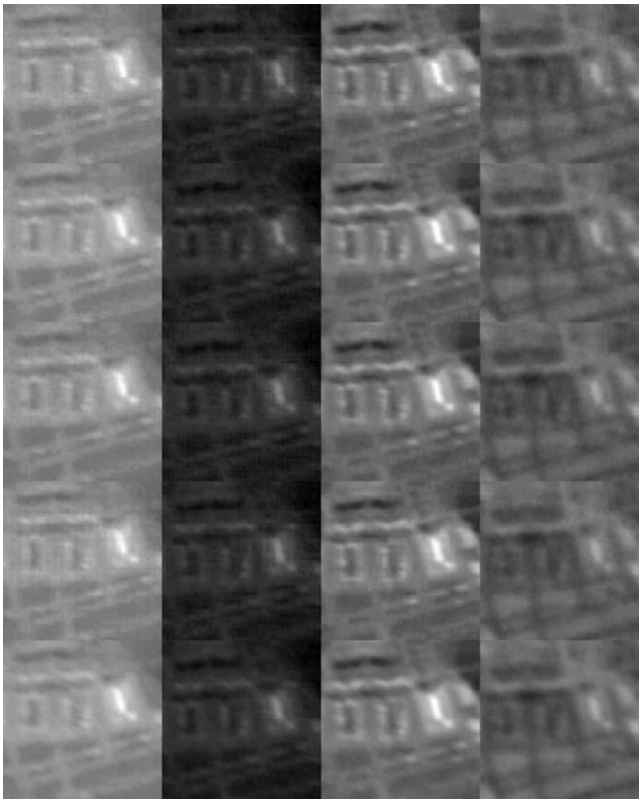

Fig. 10. Comparison among interpolations: in the first line, 5×5 interpolation, in the second 7×7 with normal correlation coefficient, in the third 7×7 interpolation with low correlation coefficient (smaller than 0.2), in the fourth algorithm of blocking reduction and in the last reconstructed images. Images with a 200% zoom.

Observe that the blocking artifact did not disappear completely, because it also affects the internal rows. Another solution can be obtained by generating five interpolated images in 5×5 blocks for each band and fusing them again. This method presents images that are more uniform and without artifacts.

4.2. CBERS-1 × Landsat-7 synthesis

For the synthesis process, the following algorithms were tested:

(a) Bayesian synthesis.
(b) Sequential projection on the lines of the matrix H, in the normal order.
(c) Sequential projection on the lines of the matrix H, in the reverse order.
(d) Projection by the least-squares method.
(e) Projection by POCS least squares.

As demonstrated by Fig. 11 the method that displayed the best results for all the four bands was projection by POCS least-squares method (e). Synthesized Band 1 tends to be more blurred because it has the smallest intersection with the panchromatic band (0.4%) and it receives a lot of influence from other bands. Band 4 has the largest intersection with the panchromatic band (53%) and for this reason it tends to give the best result for the synthesis problem.

5. Conclusions

This paper presented, to our best knowledge, the first use of POCS techniques for multispectral image data fusion. The use of POCS in the interpolation of different resolution images (CBERS-1 and Landsat-7) allowed the incorporation of super-resolution techniques in this procedure. Furthermore, the best results in the synthesis was obtained by the POCS method. The multispectral image fusion is a procedure that is difficult to compare in terms of time and efficiency because each case has its own peculiarities, as the characteristics that should be privileged or preserved in the fusion (space and spectral definition and other relationships among the interpolated pixels). The method here developed, starting from the bayesian formulation that produces synthetic images with imposed space and spectral characteristics, innovates in use of projection techniques on convex sets as in the solution of the modeled equations in the synthesis method or as in the corrections to the problems that appeared in the adaptation of the method to other geometries. To do this, some POCS

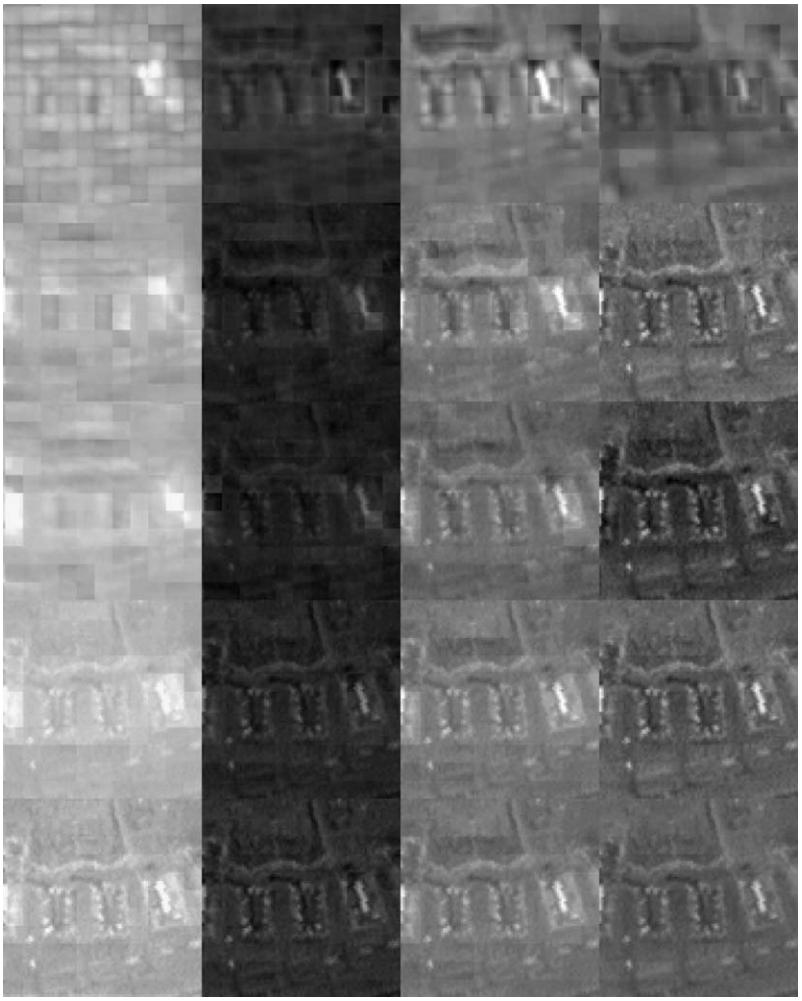

Fig. 11. Synthesis process: in the first line, result of the bayesian synthesis, in the second line sequential projection with the normal order of the matrix H, in the third line, sequential projection with reverse order with the matrix H, in fourth line the solution by the least-squares method and in fifth line the solution by the POCS least-squares method. Images with a 200% zoom.

methods used for other purposes were adapted, such as the super-resolution techniques, also used in the decompression of JPEG images [18].

We can conclude that the adaptation of the POCS and super-resolution techniques to the bayesian fusion and in the least squares solution method gives a larger flexibility in the choice of the obtained results.

In the CBERS-1 × Landsat-7 fusion, we can notice that with the help of the POCS techniques the adaptation for the new space geometry can be made and the resulting artifacts of that adaptation are softened.

The most serious limitation of the methods comes from the bayesian formulation of the problem and it consists of the necessity of overlap between the initial multispectral and panchromatic bands and the synthetic bands. We can also observe that the larger the intersection among the multispectral bands, the worse the result of the interpolation and that the larger the intersection of the multispectral and the panchromatic bands, the better result of the synthesis. That problem of choice of initial images could not be elimined by the developed methods.

Although there are limitations, there are still several POCS techniques that can be adapted to the fusion for the image improvement, such as projections in the frequency space or the use of parallel POCS techniques [20].

The interpretation of the Landsat-7 × CBERS-1 interpolation as a super-resolution technique suggests that other methods for super-resolution [21] could be applied in the image fusion problem.

Acknowledgments

The authors are grateful to Mr. Paulo R. Martini from the National Space Research Institute (INPE, Brazil) for providing the images. The work of Miss Aguena was supported by a CNPq scholarship and by a FINEP-RECOPE grant.

References

[1] R. Haydn, G.W. Dalke, J. Henkel, J.C. Bare, Application of the IHS color transform to processing of multisensor data and image enhancement in remote sensing of arid and semi-arid lands, in: Proceedings of the 1st Thematic Conference of The International Symposium on Remote Sensing of Environment, Erim, Ann Arbor, Michigan, Cairo, Egypt, January, 1992, pp. 599–616.

[2] R.E. Brum, Integration of the multispectral and panchromatic channels of the HRV (SPOT) sensor, for obtaining color composites with spatial resolution close to 10 × 10 m. MSc Thesis, 1989, (INPE-5035-TDL/403), INPE, São José dos Campos, S.P., Brazil (In Portuguese).

[3] G.F. Byrne, P.F. Crapper, K.K. Mayo, Monitoring land-cover change by principal component analysis of multitemporal Landsat-7 data, in: Remote Sensing Environment, 1980, vol. 1, pp. 887–888.

[4] J.R. Orlando, R. Mann, S. Haykin, Classification of sea-ice images using a dual -polarized radar, IEEE J. Oceanic Eng. 15 (1990) 228–237.

[5] M. Petrakos, W. Dicarlo, I. Kanellopoulos, Projection pursuit and a VR environment for visualization of remotely sensed data, in: Proceedings of the International Geoscience and Remote Sensing Symposium, IGARSS '99, 1999, vol. 5, pp. 2498–2500.

[6] S. Béthume, F. Muller, J. Donnay, Fusion of multispectral and panchromatic image by local mean and variance matching filtering techniques, in: Proceedings of The Second International Conference : Fusion of Earth Data : Merging Point Measurements, Raster Maps and Remotely Sensed Images, Sophia-Antipolis, France, 1998, pp. 31–36.

[7] B. Aiazzi, L. Alparone, S. Baronti, Quality assessment of decision-driven pyramid-based fusion of high resolution multispectral with panchromatic image data, in: Remote Sensing and Data Fusion over Urban Areas, IEEE/ISPRS Joint Workshop 2001, 2001, pp. 337–341.

[8] H. Ghassemian, Multi-sensor image fusion using multirate filter banks. in: Proceedings of the International Conference on Image Processing, 2001, vol. 1, pp. 846–849.

[9] A. Garzelli, F. Soldati, Context-driven image fusion of multispectral and panchromatic data based on a redundant wavelet representation, in: Remote Sensing and Data Fusion Over Urban Areas, IEEE/ISPRS Joint Workshop 2001, 2001, pp. 122–126.

[10] J. Núñez, X. Otazu, O. Fors, A. Prades, V. Palà, R. Arbiol, Multiresolution-based image fusion with additive wavelet decomposition, in: IEEE Transactions on Geoscience and Remote Sensing, 1999, vol. 37, No. 3, pp. 1204–1211.

[11] P. Scheunders, Multispectral image fusion using local mapping techniques, in: Proceedings ICPR2000, International Conference on Pattern Recognition, Barcelona, Spain, 2000, vol. 2, pp. 2311–2315.

[12] R.B. Gomez, A. Jazaeri, M. Kafatos, Wavelet-based hyperspectral and multispectral image fusion, SPIE's OE/Aerospace Sensing, Geo-Spatial Image and Data Exploitation II, Orlando, 2001, pp. 16–20.

[13] N.D.A. Mascarenhas, G.J.F. Banon, L.M.G. Fonseca, Simulation of a panchromatic band by spectral linear combination of multispectral bands, in: Proceedings of the International Geoscience and Remote Sensing Symposium, Espoo, Finland, IEEE, 1991, New York, pp. 407–414.

[14] N.D.A. Mascarenhas, G.J.F. Banon, A.L.B. Candeias, Multispectral image data fusion under a bayesian approach, International Journal of Remote Sensing 17 (8) (1996) 1457–1471.

[15] J. Hill, O. Diemer, Stöver, T. Udelhoven, A local correlation approach for the fusion of remote sensing data with different spatial resolutions in forestry application, International Archives of Photogrammetry and Remote Sensing, Valadolid, Spain, 1999, vol. 32, Part 7-4-3 W6.

[16] G.T. Zaniboni, M.D.A. Mascarenhas, Fusão bayesiana de imagens utilizando coeficientes de correlação localmente adaptáveis, Anais de IX Simpósio Brasileiro de Sensoriamento Remoto, Santos, SP, 1998, CD-ROM :\sbsr\8_1350.pdf. (In Portuguese).

[17] H. Stark, Y. Yang, Vector space projections, Wiley, New York, 1998.

[18] Y. Yang, N. Galatsanos, A. Katsaggelos, Projection—based spatially adaptative reconstruction of blocks transform compressed image, IEEE Trans. Image Process. (1995) 896–908.

[19] A.M. Tekalp, M.K. Ozkan, M.I. Sezan, High-resolution image reconstruction from lower-resolution image sequences and space-varying image restoration, in: IEEE int. Conf. Acoust. Speech, Signal Process., San Francisco, CA, March 23–26, 1992, pp. III-169–172.

[20] V. Censor, S.A. Zenios, Parallel optimization – Theory, algorithms and Applications, Oxford University Press, Oxford, 1997.

[21] S.C. Park, M.K. Park, M.G. Kang, Super-resolution image reconstruction: A technical overview, IEEE Signal Processing Magazine, May 2003, vol. 20, No. 3, pp. 21–36.